Finite Elements in Analysis and Design 46 (2010) 428–437

Contents lists available at ScienceDirect

Finite Elements in Analysis and Design

journal homepage: www.elsevier.com/locate/finel

Combined hybrid method applied in the Reissner–Mindlin plate model

Bing Hu [a], Zhu Wang [b,c,*,1], Youcai Xu [a]

[a] School of Mathematics, Sichuan University, Chengdu, PR China
[b] Department of Mathematics, Virginia Polytechnic Institute and State University, Blacksburg, VA, USA
[c] School of Mathematical Sciences, University of Electronic Science and Technology of China, Chengdu, PR China

ARTICLE INFO

Article history:
Received 18 January 2009
Received in revised form
9 December 2009
Accepted 7 January 2010
Available online 16 February 2010

MSC:
65N30
74S05

Keywords:
Combined hybrid method
Reissner–Mindlin plate model
Wilson

ABSTRACT

In this paper, the combined hybrid method is applied to the Reissner–Mindlin plate model and a corresponding variational formulation is presented. Based on this combined hybrid variational formulation, we introduce the Wilson incompatible displacement mode, assumed moment modes and two types of assumed shear stress to design two quadrilateral finite elements. A series of standard numerical tests show that two new elements are free of locking and yield high performance on the coarse mesh.

© 2010 Elsevier B.V. All rights reserved.

1. Introduction

It is known that, for the Reissner–Mindlin plate bending problem, standard finite element methods always fail to give good approximations when the plate thickness t is too small. This phenomenon is known as shear locking. When t is close to 0, exact solutions of the Reissner–Mindlin plate model approach those of the Kirchhoff plate model, but C^0−finite element solutions do not behave this way.

During the past several decades, much research has been focused on how to construct a general class of finite elements which can avoid locking. The first effective work involved reduced integration and selective reduced integration techniques in the displacement mode (proposed simultaneously by Zienkiewicz et al. [24] and Pawsey and Clough [12]. This was demonstrated to be the mixed finite element method by Malkus and Hughes in [9].). However, these techniques often result in instability of elements due to spurious zero-energy modes [4]. Another effective work is the mixed/hybrid element method. According to this method, many attractive elements are constructed that can avoid locking and provide uniform approximations (see [2,5–7,11]). To improve the accuracy, linked interpolation has been studied in [3,14,21,23-25]. By introducing the linking function, this method ensures that one order higher polynomials can be used for the representation of the transverse displacement without adding additional element parameters. Several finite elements are well designed based on these methods such as MITC4 and Q4-LIM, but we still want to construct some new elements that can overcome locking and achieve higher accuracy on the coarse mesh.

In the last decade, Zhou proposed the combined hybrid finite element method for the linear elliptic problem (see [15]). This method is based on a linear combination of two dual systems of saddle point conditions, one of which is the domain-decomposed Hellinger–Reissner principle, the other is the dual to the former—primal hybrid variational principle. Through the adjustment of combined parameters, this method always yields a close approximation of the energy on coarse meshes. Analyses show this method is stable and can overcome the Poisson-locking.[2] Zhou also provided a general framework for studying how to enhance accuracy on coarse meshes. In papers [16,17], numerical examples show that combined hybrid finite elements have good numerical performance. In particular, locking in the nearly incompressible region disappears. An important key to such success is to make the additional incompatible bubbles satisfy the so-called energy compatibility condition (see [15]).

Recently, the authors of this paper applied the combined hybrid method in the Reissner–Mindlin plate model and designed

* Corresponding author at: Department of Mathematics, Virginia Polytechnic Institute and State University, Blacksburg, VA, USA.
E-mail address: wangzhu@vt.edu (Z. Wang).

[1] This author was partially supported by AFOSR Grant FA9550-08-1-0136 and NSF Grant OCE-0620464.

[2] This term is used for the problem of nearly incompressible elasticity.

0168-874X/$ - see front matter © 2010 Elsevier B.V. All rights reserved.
doi:10.1016/j.finel.2010.01.003

four kinds of quadrilateral elements (see [18]). Among them, CHWu yields the best results in numerical experiments, which is based on assumed constant shear stress, assumed constant moment modes and the incompatible mode presented by Pian and Wu (see [20]). Numerical solutions show the combined hybrid finite elements are free of shear locking; meanwhile, comparisons among results show that the performance of those elements depend heavily on the option of incompatible modes.

Following these studies, in this paper, we use the same variational formulation as CHWu but change the incompatible modes to Wilson's transversal displacement [13,22], and also construct two new quadrilateral elements. One of them is based on assumed constant shear stress, the other is designed, especially, to make shear stress satisfy the complete energy compatibility condition. By comparison with other well-established elements (MITC4 and Q4-LIM), numerical experiments show both elements are free of locking and perform well on the coarse mesh in both thin and thick plate models.

This paper is organized as follows: in Section 2, the combined hybrid variational formulation of the Reissner–Mindlin plate model is reviewed with the existence and uniqueness of the solution presented; in Section 3, we discretize the variational formulation and analyze its convergence; in Section 4, two kinds of new quadrilateral elements are given and corresponding error estimations are analyzed, respectively; in Section 5, we present the interval-contracting algorithm to determine optimal values of the combined parameters; finally, both elements are tested in Section 6.

2. Combined hybrid variational formulation

Let $\Omega\times(-t/2,t/2)$ be the region occupied by a plate, where $\Omega\subset R^2$ is a simply connected polygon and $t>0$ is the plate thickness, ω denotes the transverse displacement of the midsection of the plate and β represents the rotation of fibers normal to Ω. The original Reissner–Mindlin plate model determines ω,β as unique solutions to the following variational problem:

Find $(\omega,\beta)\in H_0^1(\Omega)\times(H_0^1(\Omega))^2$, such that

$$a(\beta,\eta)+\lambda t^{-2}(\nabla\omega-\beta,\nabla v-\eta)=(g,v),\quad \forall(v,\eta)\in H_0^1(\Omega)\times(H_0^1(\Omega))^2, \tag{2.1}$$

where

$$a(\beta,\eta)=\frac{E}{12(1-v^2)}\int_\Omega\left\{v\,\mathrm{div}\,\beta\,\mathrm{div}\,\eta+\frac{1-v}{4}\sum_{i,j=1}^{2}\left(\frac{\partial\beta_i}{\partial x_j}+\frac{\partial\beta_j}{\partial x_i}\right)\left(\frac{\partial\eta_i}{\partial x_j}+\frac{\partial\eta_j}{\partial x_i}\right)\right\}d\Omega,$$

where $(\cdot,\cdot)$ is the L^2-inner product, $\lambda=Ek/2(1+v)$ using E as Young's modulus, v as the Poisson ratio, and k as the shear correction factor (taken to be $\frac{5}{6}$), g is the scaled transverse loading function.

By introducing the shear stress $\sigma=\lambda t^{-2}(\nabla\omega-\beta)$ and moment $M=D(\varepsilon(\beta))$, the combined hybrid variational principle reads: to find $(\sigma,M,\beta,\omega)\in\Gamma\times Z\times H\times U$, such that

$$\prod_{CH}^{(\alpha_1,\alpha_2)}(\sigma,M,\beta,\omega)=\inf_{\eta,v}\sup_{\tau,m}\prod_{CH}^{(\alpha_1,\alpha_2)}(\tau,m,\eta,v), \tag{2.2}$$

where the combined hybrid energy functional

$$\prod_{CH}^{(\alpha_1,\alpha_2)}(\tau,m,\eta,v)=\sum_{\Omega_i}\int_{\Omega_i}\frac{1}{2}[a(\eta,\eta)+\lambda t^{-2}(\nabla v-\eta,\nabla v-\eta)-(g,v)]\,d\Omega_i$$
$$-b_1(\tau,v_I)-\frac{(1-\alpha_1t^2)t^2}{2\lambda}(\tau-\lambda t^{-2}(\nabla v-\eta),$$
$$\tau-\lambda t^{-2}(\nabla v-\eta))-\frac{\alpha_2}{2}d(m-D\varepsilon(\eta),m-D\varepsilon(\eta)),$$

where $\Gamma=\prod_i H(\mathrm{div},\Omega_i)$, $Z=(L(\Omega))^3$, $H=(H_0^1(\Omega))^2$, $U=\{v\in\prod_i H^1(\Omega_i): v|_{\partial\Omega_i}=0\}$, $U=U_c\oplus U_I$, $U_c=H_0^1(\Omega)/\prod_i H_0^1(\Omega_i)$ is a Lagrange multiplier space, $U_I(\Omega_i)=span\langle bubbles\rangle$, $b_1(\tau,v_I)=\sum_i\oint_{\partial\Omega_i}\tau\cdot\vec{n}\cdot v_I\,ds$, $d(M,m)=\int_\Omega M\cdot D^{-1}m\,d\Omega$, D is the elasticity module matrix, $\varepsilon(\beta)=[\partial\beta_x/\partial x,\partial\beta_y/\partial y,\partial\beta_x/\partial y+\partial\beta_y/\partial x]^T$, $\alpha_1\in(0,t^{-2})$, $\alpha_2\in(0,1)$ are combined parameters, $\mathcal{T}_h=\{\Omega_i\}$ denotes the finite element regular subdivision of Ω.

By using the optimality conditions on (2.2), assuming $\omega\in C^0(\Omega)$ and $\lambda=1$ for simplicity of notation, we get the following combined hybrid variational formulation:

Find $(\sigma,M,\beta,\omega)\in\Gamma\times Z\times H\times U$, such that

$$(1-\alpha_2)a(\beta,\eta)+\alpha_1\sum_i(\nabla\omega-\beta,\nabla v-\eta)_{\Omega_i}+(1-\alpha_1t^2)\sum_i(\sigma,\nabla v-\eta)_{\Omega_i}$$
$$+\alpha_2(M,\varepsilon(\eta))-b_1(\sigma,v_I)=(g,v),\quad\forall(\eta,v)\in H\times U, \tag{2.3}$$

$$(1-\alpha_1t^2)t^2(\sigma,\tau)-(1-\alpha_1t^2)\sum_i(\tau,\nabla\omega-\beta)_{\Omega_i}+\alpha_2d(M,m)-\alpha_2(m,\varepsilon(\beta))$$
$$+b_1(\tau,\omega_I)=0,\quad\forall(\tau,m)\in\Gamma\times Z. \tag{2.4}$$

Here, H and Z are equipped with the general norm $\|\cdot\|_{1,\Omega}$ and $\|\cdot\|_{0,\Omega}$ [8], Γ and $U\times U_c$ can be equipped with the norms:

$$\|\tau\|_\Gamma=\left[\|\tau\|_{0,\Omega}^2+\sum_i h_i^2\|\mathrm{div}\,\tau\|_{0,\Omega}^2\right]^{1/2},$$
$$\|(v,v_c)\|_{U\times U_c}=\left[\sum_i\left(\|\nabla v\|_{0,\Omega_i}^2+\|v-v_c\|_{1/2,\partial\Omega_i}^2\right)\right]^{1/2},$$
$$\|v\|_{1/2,\partial\Omega_i}=\inf_{u\in H_0^1(\Omega_i)}[h_i^{-2}\|v+u\|_{0,\Omega_i}^2+\|\nabla(v+u)\|_{0,\Omega_i}^2]^{1/2},$$

where h_i denotes the diameter of Ω_i.

Lemma 2.1. *For the problem* (2.3), (2.4), *there exists a unique solution* $(\sigma,M,\beta,\omega)\in\Gamma\times Z\times H\times U$.

Proof. It is obvious that the solution to the original differential formulation of Reissner–Mindlin plate model is the solution to (2.3), (2.4).

Let $g=0$, $\eta=\beta$, $\tau=\sigma$, $m=M$, $v=\omega$, $v_I=\omega_I$ in Eqs. (2.3), (2.4), then we have

$$(1-\alpha_2)a(\beta,\beta)+\alpha_1\sum_i\|\nabla\omega-\beta\|_{0,\Omega_i}^2+(1-\alpha_1t^2)t^2(\sigma,\sigma)+\alpha_2d(M,M)=0, \tag{2.5}$$

which implies that: $\beta=0$, $\sigma=0$, $M=0$ in Ω and $\nabla\omega|_{\Omega_i}=0$.

Now plugging these values into (2.3), we get: $b_1(\tau,\omega_I)=0$ for every $\tau\in\Gamma$, where $\omega_I=\omega-\omega_c$. Since $(\omega,\omega_c)\in U\times U_c$, we have $\omega\in H_0^1(\Omega)$. Then $\omega=0$ in Ω and $\omega_I|_{\partial\Omega_i}=0$ can be derived directly (see [15]) . Thus, the existence and uniqueness are proved. □

3. Discretization and convergence

This section is to derive the discretized scheme of (2.3), (2.4) and analyzes its convergence.

Let Γ^h, Z^h, H^h, and U^h be the finite element spaces associated with the domain partition $\mathcal{T}_h$ such that $\Gamma^h\subset\Gamma$, $Z^h\subset Z$, $H^h\subset H$, and $U^h\subset U$, then (2.3), (2.4) can be discretized as follows:

Find $(\sigma_h,M_h,\beta_h,\omega_h)\in\Gamma^h\times Z^h\times H^h\times U^h$, such that

$$(1-\alpha_2)a(\beta_h,\eta)+\alpha_1\sum_i(\nabla\omega_h-\beta_h,\nabla v-\eta)_{\Omega_i}+(1-\alpha_1t^2)\sum_i(\sigma_h,\nabla v-\eta)_{\Omega_i}$$
$$+\alpha_2(M_h,\varepsilon(\eta))-b_1(\sigma_h,v_I)=(g,v),\quad\forall(\eta,v)\in H^h\times U^h, \tag{3.1}$$

$$(1-\alpha_1t^2)t^2(\sigma_h,\tau)-(1-\alpha_1t^2)\sum_i(\tau,\nabla\omega_h-\beta_h)_{\Omega_i}+\alpha_2d(M_h,m)$$
$$-\alpha_2(m,\varepsilon(\beta_h))+b_1(\tau,\omega_{h_I})=0,\quad\forall(\tau,m)\in\Gamma^h\times Z^h. \tag{3.2}$$

Remark 1. When the plate is homogeneous and isotropic rectangular and meshed by a rectangular mesh $\mathcal{T}_h$, $b_1(\tau_h, v_I)=0$, the proposed discrete schemes collapse the formulation proposed in [1].

As to existence, uniqueness and convergence of solutions to the above problem, we have the following theorem:

Theorem 3.1. *Assume $(\sigma, M, \beta, \omega)$ is the exact solution to the original differential scheme of the Reissner–Mindlin plate problem after introducing the shear stress σ and moment M. Then the problem described by* (3.1), (3.2) *has a unique solution $(\sigma_h, M_h, \beta_h, \omega_h) \in \Gamma^h \times Z^h \times H^h \times U^h$ and*

$$\|\sigma-\sigma_h\|_{0,\Omega}+\|M-M_h\|_{0,\Omega}+\|\beta-\beta_h\|_{1,\Omega}+\left(\sum_i \|\nabla(\omega-\omega_h)\|^2_{0,\Omega_i}\right)^{1/2}$$
$$\le C\left\{\inf_{\tau\in\Gamma}\|\sigma-\tau\|_{\Gamma}+\inf_{m\in Z^h}\|M-m\|_{0,\Omega}+\inf_{\eta\in H^h}\|\beta-\eta\|_{1,\Omega}\right.$$
$$\left.+\inf_{v\in U^h}\left[\sum_i\left(\|\nabla(\omega-v)\|^2_{0,\Omega_i}+\|v_I\|^2_{1/2,\partial\Omega_i}\right)\right]^{1/2}\right\}, \tag{3.3}$$

where $C>0$ is a constant independent of h.

Proof. From (3.1) and (3.2), the term $(1-\alpha_2)a(\eta,\eta)+\alpha_1\sum_i(\nabla v-\eta, \nabla v-\eta)_{\Omega_i}+(1-\alpha_1 t^2)t^2(\tau,\tau)+\alpha_2 d(m,m)$ is coercive in $\Gamma^h\times Z^h\times H^h\times U^h$, thus the existence and uniqueness of the finite element solution can be derived according to the Lax–Milgram theorem. By using the same technique as in the proof of Theorem 3.1 in [15], (3.3) can be easily proved. □

4. New elements

In this section, we will introduce the Wilson incompatible mode, assumed shear stress and moment modes to design two new combined hybrid finite elements.

4.1. Assumed incompatible modes

Let U^h_w, the Wilson's quadrilateral element space, be a substitution of U^h, i.e.

$$U^h_w := \{v\in U : v|_{\Omega_i}=(v_c+v_I)|_{\Omega_i}=(\hat{v}_c+\hat{v}_I)\circ F_i^{-1}, \forall\Omega_i\in\mathcal{T}_h\},$$
$$\hat{v}_c(\xi,\eta)=v_c(F_i(\xi,\eta))=[N_1\ \ N_2\ \ N_3\ \ N_4]X_c^{(v)}=:N_cX_c^{(v)},$$
$$\hat{v}_I=[1-\xi^2\ \ 1-\eta^2]X_I^{v}=:N_IX_I^{(v)},\quad X_I^{(v)}\in R^2, \tag{4.1}$$

where $X_c^{(v)}=(v_1,v_2,v_3,v_4)^T$ is the nodal transverse displacement vector, $N_j=\frac{1}{4}(1+\xi_j\xi)(1+\eta_j\eta)$ with (ξ_j,η_j) $(j=1,2,3,4)$ be vertices $(-1,-1),(1,-1),(1,1),(-1,1)$. F_i is the isoparametric mapping from the reference element $[-1,1]\times[-1,1]$ to Ω_i (see Fig. 1), i.e.

$$\begin{pmatrix}x\\y\end{pmatrix}=F_i(\xi,\eta)=\sum_{j=1}^{4}N_i(\xi,\eta)\begin{pmatrix}x_i\\y_i\end{pmatrix},$$

(x_j,y_j) $(j=1,2,3,4)$ are coordinates of four vertices on Ω_i.

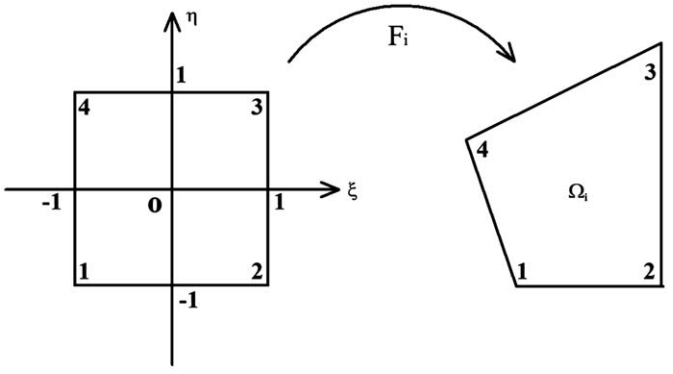

Fig. 1. Bilinear isoparameter mapping F_i.

4.2. Assumed shear resultant field

Two different types of assumed shear stress spaces, Γ_0^h and Γ_{0-1}^h, are used in this paper as follows:

$$\Gamma_0^h := \{\tau\in\Gamma : \tau|_{\Omega_i}=constant,\ \forall\Omega_i\in\mathcal{T}_h\},\ \text{i.e.}$$
$$\tau|_{\Omega_i}=\begin{bmatrix}1&0\\0&1\end{bmatrix}X^{(\tau)}=:S_0X^{(\tau)},\quad X^{(\tau)}\in R^2, \tag{4.2}$$

$$\Gamma_{0-1}^h := \{\tau\in\Gamma_1^h : b_1(\tau,v_I)=0,\ \forall v\in U_w^h\},$$
$$\Gamma_1^h := \{\tau\in\Gamma : \tau|_{\Omega_i}=\hat{p}_1\circ F_i^{-1},\ \forall\Omega_i\in\mathcal{T}_h\},$$
$$\hat{p}_1(\xi,\eta)=\begin{bmatrix}1&\xi&\eta&0&0&0\\0&0&0&1&\xi&\eta\end{bmatrix}X^{(\tau)}=:S_1X^{(\tau)},\quad X^{(\tau)}\in R^6, \tag{4.3}$$

Obviously, Γ_0^h is a constant shear resultant field and Γ_{0-1}^h, as a constrained subspace of Γ_1^h, satisfies complete energy compatibility condition (see [15]):

$$b(\tau,v_I)=\oint_{\partial\Omega_i}\tau\cdot\vec{n}\cdot v_I\,ds=0,\quad \forall v_I\in U_w^h, \tag{4.4}$$

where

$$v_I(F_i(\xi,\eta))=\hat{v}_I(\xi,\eta)=[1-\xi^2\ \ 1-\eta^2]X_I^{(v)},\quad X_I^{(v)}\in R^2$$

and

$$\tau(F_i(\xi,\eta))=\hat{\tau}(\xi,\eta)=\begin{bmatrix}1&\xi&\eta&0&0&0\\0&0&0&1&\xi&\eta\end{bmatrix}X^{(\tau)},\quad X^{(\tau)}\in R^6.$$

Therefore, according to $b(\tau,v_I)=\oint_{\partial\Omega_i}\tau\cdot\vec{n}\cdot v_I\,ds=(\mathrm{div}\,\tau,v_I)_{\Omega_i}+(\tau,\nabla v_I)_{\Omega_i}=0$, we can eliminate two parameters. Then the shear stress $\tau\in\Gamma_{0-1}^h$ can be expressed alternatively in the matrix form generated by four independent parameters, as follows:

(1) if $a_1b_3\neq0$,

$$\tau|_{\Omega_i}=\hat{\tau}\circ F_i^{-1},\hat{\tau}(\xi,\eta)=\begin{bmatrix}1-\frac{b_2}{b_3}\xi&\eta&\frac{a_2}{b_3}\xi&\frac{a_3}{b_3}\\ \frac{b_2}{a_1}\eta&\frac{b_1}{a_1}\eta&1-\frac{a_2}{a_1}\eta&\xi\end{bmatrix}X^{(\tau)}$$
$$=:S_{0-1}X^{(\tau)},\quad X^{(\tau)}\in R^4, \tag{4.5}$$

(2) if $a_3b_1\neq0$,

$$\tau|_{\Omega_i}=\hat{\tau}\circ F_i^{-1},\hat{\tau}(\xi,\eta)=\begin{bmatrix}1-\frac{b_2}{b_1}\eta&\xi&\frac{a_2}{b_1}\eta&\frac{a_1}{b_1}\eta\\ \frac{b_2}{a_3}\xi&\frac{b_3}{a_3}\xi&1-\frac{a_2}{a_3}\xi&\eta\end{bmatrix}X^{(\tau)}$$
$$=:S_{0-1}X^{(\tau)},\quad X^{(\tau)}\in R^4, \tag{4.6}$$

where $a_1=\frac{1}{4}(-x_1+x_2+x_3-x_4)$, $a_2=\frac{1}{4}(x_1-x_2+x_3-x_4)$, $a_3=\frac{1}{4}(-x_1-x_2+x_3+x_4)$; $b_1=\frac{1}{4}(-y_1+y_2+y_3-y_4)$, $b_2=\frac{1}{4}(y_1-y_2+y_3-y_4)$, $b_3=\frac{1}{4}(-y_1-y_2+y_3+y_4)$.

Remark 2. For a proper quadrilateral subdivision $\mathcal{T}_h$, cases (1) and (2) do not occur at the same time, thus (4.6) is not necessarily needed in coding (see [16]).

4.3. Assumed moment modes

We will assume moment modes to be constant, that is, Z^h is supposed to be

$$Z_0^h := \{m \in Z : m|_{\Omega_i} = constant,\ \forall \Omega_i \in \mathcal{T}_h\},\ \text{i.e.}$$
$$m|_{\Omega_i} = \begin{bmatrix} 1 & 0 & 0 \\ 0 & 1 & 0 \\ 0 & 0 & 1 \end{bmatrix} X^{(m)} =: E_0 X^{(m)}, \quad X^{(m)} \in R^3. \tag{4.7}$$

4.4. New elements

Utilizing discretized variational formulations (3.1) and (3.2), we design two new quadrilateral elements as follows:

(I) CHRM(0,0) defined on

$$\Gamma^h = \Gamma_0^h, \quad Z^h = Z_0^h, \quad U^h = U_w^h,$$
$$H^h = \{\eta \in H; \eta|_{\Omega_i} = (Q_1(\Omega_i))^2, \forall \Omega_i \in \mathcal{T}_h\};$$

(II) CHRM(0–1,0) defined on

$$\Gamma^h = \Gamma_{0-1}^h, \quad Z^h = Z_0^h, \quad U^h = U_w^h,$$
$$H^h = \{\eta \in H; \eta|_{\Omega_i} = (Q_1(\Omega_i))^2, \forall \Omega_i \in \mathcal{T}_h\},$$

where H^h is the bilinear quadrilateral element space, $\Omega_i \in \mathcal{T}_h$ is a quadrilateral subdivision of Ω.

4.4.1. Error estimation of CHRM(0,0)

In order to estimate the error of the solution to the combined hybrid element (I), we introduce a condition on the mesh subdivision.

Condition (B) (*see Shi [13]*). The distance d_{Ω_i} between the midpoints of the diagonals of quadrilateral $\Omega_i \in \mathcal{T}_h$ is of order $O(h_i^2)$ uniformly for all elements as $h_i \to 0$.

Theorem 4.1. *Assume that* $\omega \in H_0^1(\Omega) \cap H^3(\Omega)$, $\beta \in (H_0^1(\Omega) \cap H^2(\Omega))^2$, *and Condition* (B) *is satisfied, then the unique solution determined by CHRM*(0,0) *to the problems* (3.1) *and* (3.2), $(\sigma_h, M_h, \beta_h, \omega_h) \in \Gamma_0^h \times Z^h \times H^h \times U_w^h$, *satisfies*

$$t\|\sigma-\sigma_h\|_{0,\Omega} + \|\beta-\beta_h\|_{1,\Omega} + \|M-M_h\|_{0,\Omega} + \left(\sum_i \|\nabla(\omega-\omega_h)-(\beta-\beta_h)\|_{0,\Omega_i}^2\right)^{1/2}$$
$$\le C\Big\{h\|\beta\|_{2,\Omega} + (h^2+h^2/t)(\|\omega\|_{3,\Omega} + \|\beta\|_{2,\Omega}) + h(1+t)\|\sigma\|_{1,\Omega}$$
$$+ h\|\mathrm{div}\,\sigma\|_{0,\Omega} + h\|M\|_{1,\Omega} + (h^2/t)\|\omega\|_{2,\Omega}\Big\}. \tag{4.8}$$

Proof. Firstly, we suppose that $(\Pi_0\beta, \Pi_1\omega, \Pi_2\sigma, \Pi_3 M) \in H^h \times U_w^h \times \Gamma^h \times Z^h$ is any interpolated approximation of $(\beta, \omega, \sigma, M)$.

Setting $\eta = \delta\beta_h := \Pi_0\beta - \beta_h, v = \delta\omega_h := \Pi_1\omega - \omega_h, \tau = \delta\sigma_h := \Pi_2\sigma - \sigma_h$, $m = \delta M_h := \Pi_3 M - M_h$; subtracting Eqs. (3.1) and (3.2), respectively, from (2.3) and (2.4); and noticing $\omega_I|_{\partial\Omega_i} = 0$, we have

$$\Sigma_1 := (1-\alpha_2)a(\delta\beta_h, \delta\beta_h) + \alpha_1 \sum_i \|\nabla(\delta\omega_h) - \delta\beta_h\|_{0,\Omega_i}^2$$
$$+ (1-\alpha_1 t^2)t^2\|\delta\sigma_h\|_{0,\Omega}^2 + \alpha_2 d(\delta M_h, \delta M_h)$$
$$= I_1 + I_2 + I_3 + I_4 + I_5,$$

where

$$I_1 := (1-\alpha_2)a(\Pi_0\beta-\beta, \delta\beta_h) + \alpha_1 \sum_i (\nabla(\Pi_1\omega-\omega) - (\Pi_0\beta-\beta), \nabla(\delta\omega_h)$$
$$-\delta\beta_h)_{\Omega_i} + (1-\alpha_1 t^2)t^2(\Pi_2\sigma-\sigma, \delta\sigma_h) + \alpha_2 d(\Pi_3 M - M, \delta M_h),$$
$$I_2 := (1-\alpha_1 t^2)\sum_i (\Pi_2\sigma-\sigma, \nabla(\delta\omega_h) - \delta\beta_h)_{\Omega_i} + \alpha_2(\Pi_3 M - M, \varepsilon(\delta\beta_h)),$$
$$I_3 := -(1-\alpha_1 t^2)\sum_i (\delta\sigma_h, \nabla(\Pi_1\omega-\omega) - (\Pi_0\beta-\beta))_{\Omega_i} - \alpha_2(\delta M_h, \varepsilon(\Pi_0\beta-\beta)),$$
$$I_4 := b_1(\delta\sigma_h, (\Pi_1\omega)_I),$$
$$I_5 := -b_1(\Pi_2\sigma-\sigma, (\delta\omega_h)_I).$$

By using the Schwarz inequality, we have

$$I_1 \le C\left\{\|\Pi_0\beta-\beta\|_1 + \left(\sum_i \|\nabla(\Pi_1\omega-\omega) - (\Pi_0\beta-\beta)\|_{0,\Omega_i}^2\right)^{1/2}\right.$$
$$\left. + \|\Pi_3 M - M\|_{0,\Omega} + t\|\Pi_2\sigma-\sigma\|_{0,\Omega}\right\} \times (\Sigma_1)^{1/2},$$
$$I_2 \le C(\|\Pi_2\sigma-\sigma\|_{0,\Omega} + \|\Pi_3 M - M\|_{0,\Omega})$$
$$\times \left(\alpha_1 \sum_i \|\nabla(\delta\omega_h) - \delta\beta_h\|_{0,\Omega_i}^2 + (1-\alpha_2)a(\delta\beta_h, \delta\beta_h)\right)^{1/2},$$
$$I_3 \le C \times (1/t)\left(\left(\sum_i \|\nabla(\Pi_1\omega-\omega) - (\Pi_0\beta-\beta)\|_{0,\Omega_i}^2\right)^{1/2} + \|\Pi_0\beta-\beta\|_1\right)$$
$$\times ((1-\alpha t^2)t^2\|\delta\sigma_h\|_{0,\Omega}^2 + \alpha_2 d(\delta M_h, \delta M_h))^{1/2},$$
$$I_4 \le C \times (1/t)\sup_{\delta\sigma_h}(b_1(\delta\sigma_h, (\Pi_1\omega)_I)/\|\delta\sigma_h\|_\Gamma) \times (\Sigma_1)^{1/2},$$
$$I_5 \le C\|\Pi_2\sigma-\sigma\|_\Gamma \times (\Sigma_1)^{1/2}.$$

Then it is easy to check

$$(\Sigma_1)^{1/2} \le C\left\{\|\Pi_0\beta-\beta\|_1 + (1+1/t)\left(\sum_i \|\nabla(\Pi_1\omega-\omega) - (\Pi_0\beta-\beta)\|_{0,\Omega_i}^2\right)^{1/2}\right.$$
$$+ (1+t)\|\Pi_2\sigma-\sigma\|_{0,\Omega} + \|\Pi_2\sigma-\sigma\|_\Gamma + \|\Pi_3 M - M\|_{0,\Omega}$$
$$\left. + (1/t)\sup_{\delta\sigma_h}(b_1(\delta\sigma_h, (\Pi_1\omega)_I)/\|\delta\sigma_h\|_\Gamma)\right\}.$$

By the triangle inequality, we get

$$\|\beta-\beta_h\|_{1,\Omega} + \left(\sum_i \|\nabla(\omega-\omega_h) - (\beta-\beta_h)\|_{0,\Omega_i}^2\right)^{1/2} + t\|\sigma-\sigma_h\|_{0,\Omega} + \|M-M_h\|_{0,\Omega}$$
$$\le C\left\{\|\Pi_0\beta-\beta\|_1 + (1+1/t)\left(\sum_i \|\nabla(\Pi_1\omega-\omega) - (\Pi_0\beta-\beta)\|_{0,\Omega_i}^2\right)^{1/2}\right.$$
$$+ \|\Pi_3 M - M\|_{0,\Omega} + (1+t)\|\Pi_2\sigma-\sigma\|_{0,\Omega} + \|\Pi_2\sigma-\sigma\|_\Gamma$$
$$\left. + (1/t)\sup_{\tau \in \Gamma^h}(b_1(\tau, (\Pi_1\omega)_I)/\|\tau\|_\Gamma)\right\}.$$

Since condition (B) is satisfied on the mesh subdivision, considering Propositions 3.1 and 4.1 in [15], we have

$$\sup_{\tau \in \Gamma^h}(b_1(\tau, (\Pi_1\omega)_I)/\|\tau\|_\Gamma) \le Ch^2\|\omega\|_{2,\Omega}.$$

Using the interpolation estimate, we have

$$t\|\sigma-\sigma_h\|_{0,\Omega} + \|\beta-\beta_h\|_{1,\Omega} + \|M-M_h\|_{0,\Omega} + \left(\sum_i \|\nabla(\omega-\omega_h) - (\beta-\beta_h)\|_{0,\Omega_i}^2\right)^{1/2}$$
$$\le C\Big\{h\|\beta\|_{2,\Omega} + (h^2+h^2/t)(\|\omega\|_{3,\Omega} + \|\beta\|_{2,\Omega}) + h(1+t)\|\sigma\|_{1,\Omega}$$
$$+ h\|\mathrm{div}\,\sigma\|_{0,\Omega} + h\|M\|_{1,\Omega} + (h^2/t)\|\omega\|_{2,\Omega}\Big\}. \qquad \square$$

4.4.2. Error estimation of CHRM(0–1,0)

Lemma 4.1. *It is obvious that*

$$b_1(\tau, v_I) = 0, \quad \forall \tau \in \Gamma_{0-1}^h,\ v \in U_w^h.$$

As for the combined hybrid element (II), we have the following error estimate:

Theorem 4.2. *If* $\omega \in H_0^1(\Omega)\cap H^3(\Omega)$ *and* $\beta \in (H_0^1(\Omega)\bigcap H^2(\Omega))^2$, *the unique solution determined by CHRM*(0–1,0) *to the problems* (3.1) *and* (3.2), $(\sigma_h, M_h, \beta_h, \omega_h) \in \Gamma_0^h \times Z^h \times H^h \times U_w^h$, *satisfies*

$$t\|\sigma-\sigma_h\|_{0,\Omega}+\|\beta-\beta_h\|_{1,\Omega}+\|M-M_h\|_{0,\Omega}+\left(\sum_i \|\nabla(\omega-\omega_h)-(\beta-\beta_h)\|_{0,\Omega_i}^2\right)^{1/2}$$
$$\le C\Big\{h\|\beta\|_{2,\Omega}+(h^2+h^2/t)(\|\omega\|_{3,\Omega}+\|\beta\|_{2,\Omega})+h(1+t)\|\sigma\|_{1,\Omega}$$
$$+h\|\operatorname{div}\sigma\|_{0,\Omega}+h\|M\|_{1,\Omega}\Big\}. \quad (4.9)$$

Proof. From Lemma 4.1, the I_4 term in the proof of Theorem 4.1 equals zero. Then the error estimate is easy to obtain. □

5. Optimal combined parameters

It is known that combined hybrid finite elements can achieve highly accurate estimates of energy on coarse meshes by adjusting the parameters [15–17], which makes combined hybrid elements competitive comparing with other well-established elements. In this section, we will discuss how to choose the optimal values of these parameters, α_1^* and α_2^*.

Assume that $(\sigma_H, M_H, \beta_H, \omega_H)$ is the solution to (2.3), (2.4) on the coarse mesh with mesh size H. First consider (2.2),

$$\prod_{CH}^{(\alpha_1,\alpha_2)}(\sigma_H, M_H, \beta_H, \omega_H)=\inf_{\eta,\nu}\sup_{\tau,m}\prod_{CH}^{(\alpha_1,\alpha_2)}(\tau, m, \eta, \nu),$$
$$=\inf_{\eta,\nu}\Big\{\prod_P(\eta,\nu)-b_1(\tau,\nu_I)$$
$$-\inf_{\tau}\frac{(1-\alpha_1 t^2)t^2}{2\lambda}(\tau-\lambda t^{-2}(\nabla\nu-\eta),\tau-\lambda t^{-2}(\nabla\nu-\eta))$$
$$-\inf_{m}\frac{\alpha_2}{2}d(m-D\varepsilon(\eta),m-D\varepsilon(\eta))\Big\},$$

where $\prod_P(\eta,\nu)=\sum_{\Omega_i}\int_{\Omega_i}\frac{1}{2}[a(\eta,\eta)+\lambda t^{-2}(\nabla\nu-\eta,\nabla\nu-\eta)-(g,\nu)]\,d\Omega_i$. Obviously, different choices of parameters lead to different values

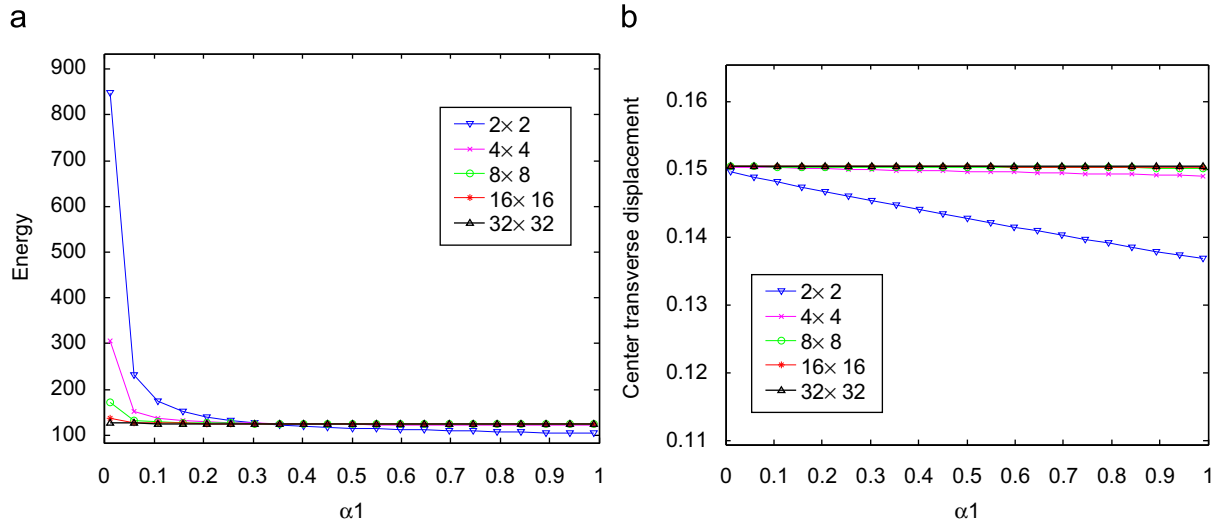

Fig. 2. At $\alpha_2=0.5$, the combined hybrid energy (left) and the displacement at the center of the plate (right) at different values of α_1 on different meshes. Notice the combined hybrid energy at different values of the parameter all converge to almost the exact solution on the 32×32 mesh; the nearly exact energy can be achieved on the 2×2 mesh at $\alpha_1^*=0.32148$.

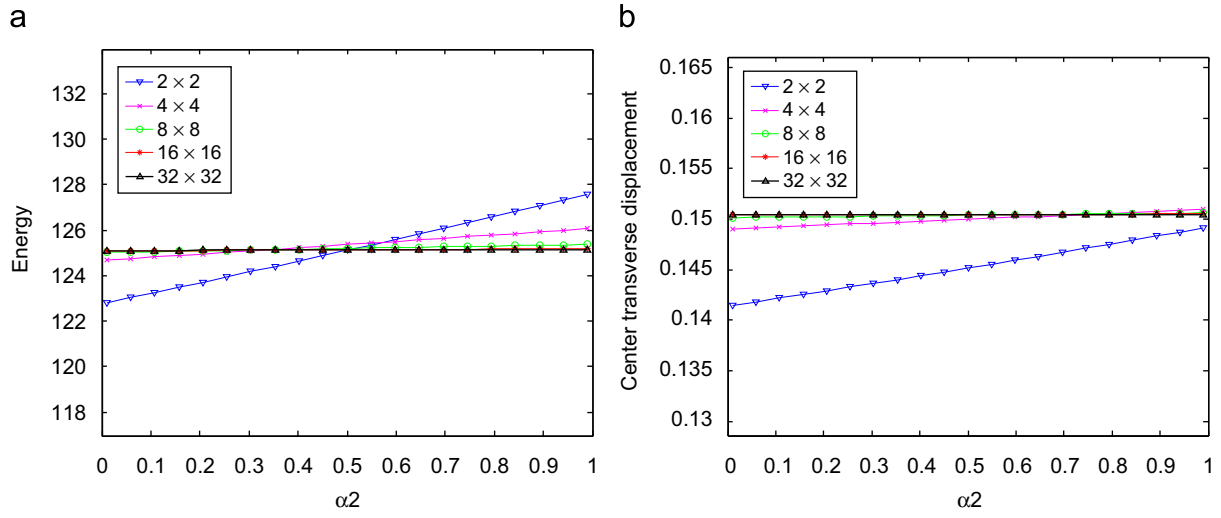

Fig. 3. At $\alpha_1^*=0.32148$, the combined hybrid energy (left) and the displacement at the center of the plate (right) at different values of α_2 on different meshes. Notice that almost the same combined hybrid energy and central displacement results are obtained on the 32×32 mesh. On the 2×2 mesh, the central transverse displacement approaches the exact solution as α_2 increases, while the combined hybrid energy increases slowly at the same time.

of the combined hybrid energy. As $b_1(\tau, v_I)=0$, if both $1-\alpha_1 t^2$ and α_2 are close to 0, the combined hybrid energy, $\prod_{CH}^{(\alpha_1,\alpha_2)}(\sigma_H, M_H, \beta_H, \omega_H)$ is always smaller than the exact energy value $\prod_{exact}$; while if $1-\alpha_1 t^2$ and α_2 are close to 1, the combined hybrid energy will always be much greater than the exact energy value since the finite element solution diverges as they approach one. Due to the continuity of parameters in the energy functional, we have:

Proposition 1. *There exist* $\alpha_1^* \in (0, t^{-2})$ *and* $\alpha_2^* \in (0,1)$ *such that*

$$\prod_{CH}^{(\alpha_1^*,\alpha_2^*)}(\sigma_H, M_H, \beta_H, \omega_H) = \prod_{exact}. \tag{5.1}$$

This shows that the combined hybrid scheme can achieve the exact energy on a coarse mesh by adjusting parameters. We believe that the optimal parameters, α_1^*, α_2^* can be determined through deeper theoretical analysis, which will be our future work. Here, we present a way to approximate them in the application by implementing the interval-contracting algorithm (Algorithm 1).

To illustrate the idea, we take the square plate, whose thickness is 1, with uniform load and clamped boundary for example. We apply the element CHRM(0, 0). First set $\alpha_2 = 0.5$, and then solve (2.3)–(2.4) on different meshes, respectively, with α_1 varying from 0.01 to 0.99 by adding a constant step 0.049.

Fig. 2 shows the combined hybrid energy (left) and the displacement at the center of the plate (right) at different values of α_1 on different meshes. As 32×32 mesh is utilized, the combined hybrid energy values at different α_1 are all close to the exact energy, which, on the one hand, shows the combined hybrid method is stable for a large range of parameters; on the other hand, this shows that the combined hybrid energy on the 32×32 mesh at any parameter can be regard as a criterion (the combined hybrid energy converges to the almost exact energy). The optimal parameter can be found by comparing the combined hybrid energy on the 2×2 mesh with the criterion. When a 2×2 mesh is used, the optimal value of α_1 is located at [0.3, 0.4] (close to the intersection of the blue curve and the black one). By implementing Algorithm 1, we get a good estimate of $\alpha_1^* = 0.32148$. Using α_1^* and keeping $\alpha_2 = 0.5$ causes a loss of accuracy in the central displacement. We will improve it by adjusting the value of α_2 in the next step.

Secondly, we fix $\alpha_1 = \alpha_1^*$ and solve (2.3)–(2.4) on different meshes with α_2 varying from 0.01 to 0.99, respectively, by adding the constant step 0.049. Fig. 3 shows the combined hybrid energy (left) and the displacement at the center of the plate (right) at different values of α_2 on different meshes. Notice almost same combined hybrid energy and central displacement results are obtained on the 32×32 mesh. On the coarse 2×2 mesh, the central transverse displacement approaches the exact solution as α_2 increases, while the combined hybrid energy increases slowly at the same time. We can use this property to balance the accuracy of the energy and the central displacement on the coarse mesh. For instance, we adjust α_2 to achieve higher accuracy for the central displacement and retain

$$\frac{\prod_{CH}^{(\alpha_1^*,\alpha_2^*)}(\sigma_H, M_H, \beta_H, \omega_H)}{\prod_{CH}^{(\alpha_1^*,0.5)}(\sigma_H, M_H, \beta_H, \omega_H)} \in [0.99, 1.01].$$

By implementing Algorithm 1, we find $\alpha_2^* = 0.75308$.

In the following, we describe the interval-contracting algorithm.

Algorithm 1. Interval-contracting algorithm.

Input: $\alpha_1^c = 0.5t^2$, $\alpha_2^c = 0.5$
Output: α_1^*, α_2^*

Set $\alpha_1^0 = \alpha_1^c$, $T = t^{-2}$, compute $\mathcal{E}_e^{(\alpha_1^0)} = \mathcal{E}_e^{(\alpha_1^0,\alpha_2^c,\alpha_1^c,\alpha_2^c)}$, and compute $\Delta\alpha(\mathcal{E}_e^{(\alpha_1^0)}) = \Delta\alpha(\mathcal{E}_e^{(\alpha_1^0,\alpha_2^c,\alpha_1^c,\alpha_2^c)}, T)$;
while $|\mathcal{E}_e^{(\alpha_1^0)}| > 10^{-3}$ & $|\Delta\alpha(\mathcal{E}_e^{(\alpha_1^0)})| > 10^{-4}$ **do**
  $\alpha_1^1 = \alpha_1^0 + \Delta\alpha(\mathcal{E}_e^{(\alpha_1^0)})$;
  if $\mathrm{sign}(\mathcal{E}_e^{(\alpha_1^1)}) = -\mathrm{sign}(\mathcal{E}_e^{(\alpha_1^0)})$ **then**
    reset $\Delta\alpha(\mathcal{E}_e^{(\alpha_1^1)}) = \frac{|\alpha_1^1-\alpha_1^0|}{2}\cdot \mathrm{sign}(\mathcal{E}_e^{(\alpha_1^1)})$;
  $\alpha_1^0 = \alpha_1^1$;
$\alpha_1^* = \alpha_1^0$;
Set $\alpha_2^0 = \alpha_2^c$, $T = 1$, compute $\mathcal{E}_\omega^{(\alpha_2^0)} = \mathcal{E}_\omega^{(\alpha_1^*,\alpha_2^0,\alpha_1^c,\alpha_2^c)}$, and compute $\Delta\alpha(\mathcal{E}_\omega^{(\alpha_2^0)}) = \Delta\alpha(\mathcal{E}_\omega^{(\alpha_1^*,\alpha_2^0,\alpha_1^c,\alpha_2^c)}, T)$;
while $|\mathcal{E}_\omega^{(\alpha_2^0)}| > 10^{-3}$ & $|\Delta\alpha(\mathcal{E}_\omega^{(\alpha_2^0)})| > 10^{-4}$ & $|1-\prod_{CH}^{(\alpha_1^*,\alpha_2^0)} / \prod_{CH}^{(\alpha_1^*,\alpha_2^c)}| \le 0.01$ **do**
  $\alpha_2^1 = \alpha_2^0 + \Delta\alpha(\mathcal{E}_\omega^{(\alpha_2^0)})$;
  if $\mathrm{sign}(\mathcal{E}_\omega^{(\alpha_2^1)}) = -\mathrm{sign}(\mathcal{E}_\omega^{(\alpha_2^0)})$ **then**
    reset $\Delta\alpha(\mathcal{E}_\omega^{(\alpha_2^1)}) = \frac{|\alpha_2^1-\alpha_2^0|}{2}\cdot \mathrm{sign}(\mathcal{E}_\omega^{(\alpha_2^1)})$;
  $\alpha_2^0 = \alpha_2^1$;
$\alpha_2^* = \alpha_2^0$

Let $\prod_{CH}^{(\tilde\alpha_1,\tilde\alpha_2)}(\sigma_H, M_H, \beta_H, \omega_H)$ and $\omega_H^{(\tilde\alpha_1,\tilde\alpha_2)}$ be the energy and the central displacement on the coarse mesh (2×2); $\prod_{CH}^{(\alpha_1,\alpha_2)}(\sigma_h, M_h, \beta_h, \omega_h)$ and $\omega_h^{(\alpha_1,\alpha_2)}$ be the energy and the central displacement on the fine mesh (32×32). Let

$$\mathcal{E}_e^{(\tilde\alpha_1,\tilde\alpha_2,\alpha_1,\alpha_2)} = \frac{\prod_{CH}^{(\tilde\alpha_1,\tilde\alpha_2)}(\sigma_H, M_H, \beta_H, \omega_H) - \prod_{CH}^{(\alpha_1,\alpha_2)}(\sigma_h, M_h, \beta_h, \omega_h)}{|\prod_{CH}^{(\tilde\alpha_1,\tilde\alpha_2)}(\sigma_H, M_H, \beta_H, \omega_H) + \prod_{CH}^{(\alpha_1,\alpha_2)}(\sigma_h, M_h, \beta_h, \omega_h)|/2},$$

$$\mathcal{E}_\omega^{(\tilde\alpha_1,\tilde\alpha_2,\alpha_1,\alpha_2)} = \frac{\omega_H^{(\tilde\alpha_1,\tilde\alpha_2)} - \omega_h^{(\alpha_1,\alpha_2)}}{|\omega_H^{(\tilde\alpha_1,\tilde\alpha_2)} + \omega_h^{(\alpha_1,\alpha_2)}|/2},$$

$$\Delta\alpha(\mathcal{E}, T) = \begin{cases} \mathrm{sign}(\mathcal{E})\cdot 0.05T & |\mathrm{sign}(\mathcal{E})| < 0.03, \\ \mathrm{sign}(\mathcal{E})\cdot 0.10T & 0.03 \le |\mathrm{sign}(\mathcal{E})| \le 0.06, \\ \mathrm{sign}(\mathcal{E})\cdot 0.15T & |\mathrm{sign}(\mathcal{E})| > 0.06. \end{cases}$$

6. Numerical experiments

In this section, several standard test problems [19,23] are used to examine the new elements, CHRM(0,0) and CHRM(0–1,0). Results are compared with CHWu [18], and two other kinds of well-established element: Q4-LIM ([3]) and MITC4 ([10]) for two main purposes. One is to measure the quality of the new elements on the coarse mesh to verify that the combined hybrid method can achieve high accuracy on the coarse mesh. The other is to test the overall behavior of new elements to tell whether the Wilson displacement mode is a generally good choice or not.

For convergence criteria, the energy norm is the natural convergence test for the finite element method [19]. But it is common in the literature to examine convergence by analyzing the displacement at characteristic points such as the center of a plate. Thus, in this paper, not only the energy norm but also the transverse displacement and moment at the center of the plate are considered in the convergence test.

Table 1
Notations.

t	Thickness of plates
L	Length of a side of square plates
R	Radius of circular plates
ω_c	Transverse displacement at the center of plates
M_c	Moment at the center of plates
Energy	Twice the internal strain energy

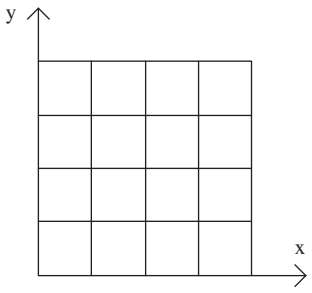

Fig. 4. $\frac{1}{4}$ square plate (16 elements).

Table 2
Material properties.

	Thin plate	Thick plate
E	10.92e+6	10.92
v	0.3	0.3
t	0.01	1
L	10.0	10.0

Table 3
Square plates: (α_1^*, α_2^*).

Boundary	Element	$t=0.01$	$t=1$
Clamped	CHRM(0,0)	(0.34857, 0.68091)	(0.32148, 0.75308)
	CHRM(0–1,0)	(0.34857, 0.68091)	(0.30508, 0.74985)
SS1	CHRM(0,0)	(2.2302, 0.50000)	(0.99906, 0.29360)
	CHRM(0–1,0)	(1.9364, 0.50000)	(0.99906, 0.29067)

Test problems contain both square plates and circular plates. Only the case of uniform loading is examined. Notations are listed in Table 1, where ω_c, M_c and Energy are functions of the number of mesh elements.

6.1. Square plates

A square plate is modeled using uniform square elements. Due to symmetry, only one quarter of the plate is discretized, and the 4×4 mesh is shown in Fig. 4. The material properties used are shown in Table 2. Optimal combined parameters used in tests are listed in Table 3.

6.1.1. Clamped boundary

Numerical results for both thin and thick plates with clamped boundary are summarized in Table 4. The exact solutions of the thin plate are $\omega_c = 12.653$, $M_c = -2.2905$ [3]. Exact solutions of the thick plate are $\omega_c = 14.99$, $M_c = -2.31$ [3].

For ω_c, when a 2×2 mesh is considered, CHWu gets the best result among three combined hybrid elements, which yields 99.50% of the exact solution for the thin plate and 100.36% of the exact value for the thick plate. Meanwhile, both CHRM(0,0) and CHRM(0–1,0) result in good performances on finer meshes. In the case of 4×4 mesh, in the thin plate, CHRM(0,0) yields 99.78% of the exact solution and CHRM(0–1,0) obtains 99.58% of it; and in the thick plate, CHRM(0,0) yields 100.38% of the exact value and CHRM(0–1,0) obtains 100.10% of that.

For M_c, both CHRM(0,0) and CHRM(0–1,0) provide a little bit more accurate results than CHWu. CHRM(0–1,0) reaches about 111.63% of exact solution of the thin plate at 2×2 mesh. And using the same mesh, both elements get about 104.97% of the exact solution on the thick plate.

Three combined hybrid finite elements all lead to excellent performance on the energy norm, which can be easily found from the tables.

In this test, on the 16×16 mesh, both new elements perform better than Q4-LIM and MITC4.

6.1.2. Simply supported boundary

Table 5 gives the numerical results for a square plate with simply supported boundary conditions (SS1, see [19]) for both thin and thick plates. The exact values for the thin plate are Energy = 425.62, $\omega_c = 40.6237$, $M_c = -4.78863$ [14].

CHRM(0–1,0) provides the best results in both cases at the 2×2 mesh, which yields 100.00% of the exact energy, 100.01% of the exact ω_c and 99.74% of the exact M_c for the thin plate problem. It also yields 99.49% of the energy, 100.04% of ω_c, 102.08% of M_c obtained on 1024 mesh elements for the thick plate.

On the 32×32 mesh, both new elements get the same good results as Q4-LIM and are better than MITC4.

6.2. Circular plates

Due to symmetry, only one quadrant of a circular plate is discretized, and a typical mesh is shown in Fig. 5. The material properties used are listed in Table 6. Optimal combined parameters used in experiments are listed in Table 7.

6.2.1. Clamped boundary

Table 8 lists numerical results for thin and thick circular plates with clamped boundary conditions. The exact solutions of the thin plate are Energy = 64.09118, $\omega_c = 9.78348$ [19], $M_c = -2.0313^+$ [23]. Exact solutions of the thick plate are Energy = 81.4471 and $\omega_c = 11.5513$ [19].

CHRM(0–1,0) provides the best results for both kinds of plates. For the thin plate, it gets 100.69% of the exact energy and 97.61% of the exact ω_c, and it also provides 103.63% of the exact M_c solution when the mesh element number is 12. In the case of the thick plate, CHRM(0–1,0) yields 100.49% of the accurate energy solution, 98.54% of the exact ω_c and 100.36% of the M_c using 768 mesh elements.

When 768 mesh elements are used, both new elements perform better than MITC4.

6.2.2. Simply supported boundary

Table 9 gives numerical results for thin and thick circular plates with simply supported (SS1) boundary conditions, respectively. The exact solutions of the thin plate are Energy = 359.08748, $\omega_c = 39.83156$ [19], $M_c = -5.1563$ [23]. Exact solutions of the thick plate are Energy = 376.4434, $\omega_c = 41.599$ [19], $M_c = -5.1563$ [3].

As for the thin plate, CHRM(0–1,0) provides the best results among the combined hybrid elements, which obtains 100.13% of the exact energy, 100.16% of exact M_c, and also provides 98.33% of the exact ω_c when the mesh element number is 12. In the case of the thick plate, CHRM(0–1,0) also gives the best results. On 12 mesh

Table 4
Clamped square plate: displacement and moments at the center.

Element	Mesh	$L/t=1000(t=0.01)$			$L/t=10(t=1)$		
		$\omega_c \Big/ \left(\frac{qL^4}{100}\right)$	$M_c \Big/ \left(\frac{qL^2}{100}\right)$	Energy	$\omega_c \Big/ \left(\frac{qL^4}{100}\right)$	$M_c \Big/ \left(\frac{qL^2}{100}\right)$	Energy
CHRM(0, 0)	2×2	0.12293	2.5568	98.1782	0.14718	2.3638	126.3658
	4×4	0.12625	2.3511	97.8587	0.15047	2.3647	125.7196
	8×8	0.12650	2.3066	97.4521	0.15050	2.3326	125.2829
	16×16	0.12653	2.2945	97.3269	0.15047	2.3232	125.1549
	32×32	0.12653	2.2915	97.2940	0.15047	2.3208	125.1218
CHRM(0–1, 0)	2×2	0.12293	2.5569	98.1778	0.14583	2.4247	126.3396
	4×4	0.12625	2.3511	97.8586	0.15005	2.3661	125.6429
	8×8	0.12650	2.3066	97.4520	0.15038	2.3319	125.2485
	16×16	0.12653	2.2945	97.3268	0.15044	2.3230	125.1448
	32×32	0.12653	2.2915	97.2940	0.15046	2.3207	125.1191
CHWu	2×2	0.12590	2.6187	98.2200	0.15044	2.3799	126.3019
	32×32	0.12653	2.2915	97.2868	0.15047	2.3208	125.1154
Q4-LIM	32×32	0.12649	2.2886	-	0.15043	2.3180	–
MITC4	33×33	0.126452	–	–	0.150366	–	–
Exact		0.12653	2.2905	–	0.1499	2.31	–

Table 5
Simply supported square plate: displacement and moments at the center.

Element	Mesh	$L/t=1000$ $(t=0.01)$			$L/t=10$ $(t=1)$		
		$\omega_c \Big/ \left(\frac{qL^4}{100}\right)$	$M_c \Big/ \left(\frac{qL^2}{100}\right)$	Energy	$\omega_c \Big/ \left(\frac{qL^4}{100}\right)$	$M_c \Big/ \left(\frac{qL^2}{100}\right)$	Energy
CHRM(0, 0)	2×2	0.40633	4.8625	425.6503	0.46168	5.2004	488.3555
	4×4	0.41539	4.9519	435.4038	0.45772	5.0819	485.2306
	8×8	0.40969	4.8594	429.3920	0.45905	5.0778	487.6600
	16×16	0.40734	4.8116	426.8477	0.46081	5.0893	489.9789
	32×32	0.40673	4.7947	426.1871	0.46145	5.0939	490.8028
CHRM(0–1, 0)	2×2	0.40626	4.7763	425.6244	0.46163	5.1997	488.3024
	4×4	0.41335	4.8710	433.0510	0.45770	5.0817	485.2119
	8×8	0.40843	4.8137	427.9318	0.45905	5.0778	487.6526
	16×16	0.40682	4.7953	426.2447	0.46081	5.0893	489.9766
	32×32	0.40641	4.7905	425.8106	0.46145	5.0939	490.8022
CHWu	2×2	0.40736	5.7038	421.3396	0.45211	6.0399	495.7852
	32×32	0.40649	4.7927	425.8887	0.46164	5.0955	491.0683
Q4-LIM	32×32	–	–	-	0.46144	5.0922	–
MITC4	33×33	0.405284	–	–	0.459240	–	–
Exact		0.40623	4.78863	425.6276			

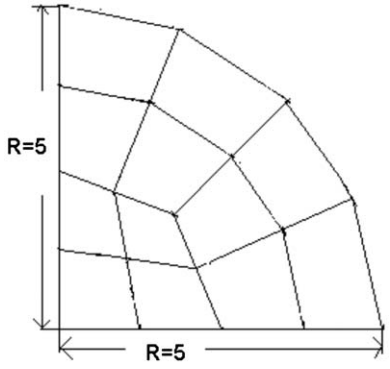

Fig. 5. $\frac{1}{4}$ circular plate (12 elements).

elements, CHRM(0–1,0) yields 100.10% of the analytical energy solution, 100.57% of the exact M_c and 98.82% of the exact ω_c.

New elements achieve almost the same results as Q4-LIM and perform better than MITC4.

Table 6
Material properties.

	Thin plate	Thick plate
E	10.92e+3	10.92
v	0.3	0.3
t	0.1	1
R	5.0	5.0

Table 7
Circular plates: (α_1^*, α_2^*).

Boundary	Element	$t=0.1$	$t=1$
Clamped	CHRM(0,0)	(0.14727, 0.99991)	(0.16571, 0.99910)
	CHRM(0–1,0)	(0.21969, 0.99985)	(0.12299, 0.99995)
SS1	CHRM(0,0)	(0.078437, 0.99995)	(0.083313, 0.99995)
	CHRM(0–1,0)	(0.092187, 0.99995)	(0.050964, 0.99985)

Table 8
Clamped circular plate: displacement and moments at the center.

Element	Mesh	$R/t=50$ $(t=0.1)$			$R/t=5$ $(t=1)$		
		$W\Big/\left(\frac{q(2R)^4}{100}\right)$	$M\Big/\left(\frac{q(2R)^2}{100}\right)$	Energy	$W\Big/\left(\frac{q(2R)^4}{100}\right)$	$M\Big/\left(\frac{q(2R)^2}{100}\right)$	Energy
CHRM(0, 0)	12	0.090426	2.0178	64.4321	0.10847	1.9749	81.7877
	48	0.095997	2.0427	64.2253	0.11368	2.0191	81.5932
	192	0.097378	2.0286	64.1309	0.11505	2.0285	81.4877
	768	0.097721	2.0306	64.1015	0.11540	2.0306	81.4575
CHRM(0–1, 0)	12	0.095498	2.1050	64.5364	0.11383	2.0398	81.8483
	48	0.097317	2.0460	64.5102	0.11507	2.0345	81.5830
	192	0.097705	2.0360	64.2117	0.11540	2.0323	81.4834
	768	0.097802	2.0332	64.1224	0.11548	2.0325	81.4563
CHWu	12	0.090879	1.9677	64.3706	0.10825	1.9320	81.8580
	768	0.097735	2.0304	64.1015	0.11541	2.0304	81.4606
Q4- LIM	768	–	–	–	–	–	–
MITC4	768	0.098158	–	–	0.116015	–	–
Exact		0.097835	2.0313^{+}	64.09118	0.115513	–	81.4471

Table 9
Simply supported circular plate: displacement and moments at the center.

Element	Mesh	$R/t=50$ $(t=0.1)$			$R/t=5$ $(t=1)$		
		$W\Big/\left(\frac{q(2R)^4}{100}\right)$	$M\Big/\left(\frac{q(2R)^2}{100}\right)$	Energy	$W\Big/\left(\frac{q(2R)^4}{100}\right)$	$M\Big/\left(\frac{q(2R)^2}{100}\right)$	Energy
CHRM(0, 0)	12	0.38522	5.1625	359.4563	0.40338	5.1185	376.8089
	48	0.39526	5.1996	359.6051	0.41296	5.1445	376.9721
	192	0.39757	5.1574	359.2481	0.41524	5.1534	376.6046
	768	0.39813	5.1556	359.1298	0.41581	5.1556	376.4434
CHRM(0–1, 0)	12	0.39165	5.1645	395.5451	0.41107	5.1856	376.8030
	48	0.39701	5.1751	360.2409	0.41480	5.1632	376.8243
	192	0.39800	5.1618	359.4383	0.41570	5.1581	376.5584
	768	0.39824	5.1602	359.1791	0.41592	5.1567	376.4735
CHWu	12	0.36500	4.8963	357.4737	0.38215	4.8573	375.4244
	768	0.39779	5.1517	359.0667	0.41547	5.1517	376.4335
Q4- LIM	768	0.39835	5.1548	-	0.41602	5.1548	–
MITC4	768	0.399063	–	–	0.41723	–	–
Exact		0.398316	5.1563	359.0875	0.41599	5.1563	376.4434

7. Conclusion

This paper presents two kinds of new elements, CHRM(0,0) and CHRM(0–1,0), for solving the Reissner–Mindlin plate model. Both elements are based on the combined hybrid variational formulation, assumed shear resultant field, assumed moment modes and Wilson's quadrilateral element space. The difference is that CHRM(0,0) uses assumed constant shear stress while CHRM(0–1) uses the constrained assumed shear stress to satisfy the complete energy compatibility condition.

Numerical results of a series of standard test problems show that both CHRM(0,0) and CHRM(0–1,0) are free of locking and yield almost the same good results as Q4-LIM on the fine mesh (and better than MITC4); but combined hybrid elements achieve higher accuracy on the coarse mesh. In particular, CHRM(0–1,0) obtains the best overall performance among the three combined hybrid elements in numerical experiments. The main reasons are:

(1) The complete energy compatibility condition [15] is fulfilled in constructing the elements, which is a guide to construct 'good' combined hybrid elements.
(2) The utilization of the Wilson incompatible displacement mode.

We present the interval-contracting algorithm to approximate optimal parameters in this paper. An analytic expression for these quantities will be studied in future work.

Acknowledgments

The authors are grateful to the reviewers for many valuable comments and helpful suggestions. Particular thanks are due to Dr. John Burkardt (Virginia Tech) for revising the language.

References

[1] D.N. Arnold, F. Brezzi, Some new elements for the Reissner–Mindlin plate model, in: J.-L. Lions, C. Baiocchi (Eds.), Boundary Value Problems for Partial Differential Equations and Applications, Masson, Paris, 1993, pp. 287–292.
[2] D.N. Arnold, R.S. Falk, A uniformly accurate finite element method for the Reissner–Mindlin plate, SIAM J. Numer. Anal. 26 (1989) 1276–1290.
[3] F. Auricchio, R.L. Taylor, A shear deformable plate element with an exact thin limit, Comput. Methods Appl. Mech. Eng. 118 (1994) 393–412.
[4] T. Belytschko, H. Stolarski, N. Carpenter, A C^0 triangular plate elements with one-point quadrature, Int. J. Numer. Methods Eng. 320 (1984) 787–802.
[5] F. Brezzi, M. Fortin, Mixed and Hybrid Finite Element Methods, Springer, Berlin, 1991.

[6] F. Brezzi, K.J. Bathe, M. Fortin, Mixed-interpolated elements for the Reissner–Mindlin plate, Int. J. Numer. Methods Eng. 28 (1989) 1787–1801.
[7] F. Brezzi, M. Fortin, Numerical approximation of Mindlin–Reissner plates, Math. Comput. 47 (1986) 151–158.
[8] P.G. Ciarlet, The Finite Element Method for Elliptic Problem, North-Holland, Amsterdam, 1978.
[9] D.S. Malkus, T.J.R. Hughes, Mixed finite element methods—reduced and selective integration techniques: a unification of concepts, Comput. Methods Appl. Mech. Eng. 15 (1) (1978) 63–81.
[10] J. Hu, Z.-C. Shi, Error analysis of quadrilateral Wilson element for the Reissner–Mindlin plate, Comput. Methods Appl. Mech. Eng. 197 (2008) 464–475.
[11] P.-B. Ming, Z.-C. Shi, Analysis of some low order quadrilateral Reissner–Mindlin plate elements, Math. Comput. 75 (2006) 1043–1065.
[12] S.F. Pawsey, R.W. Clough, Improved numerical integration for thick slab finite elements, Int. J. Numer. Methods Eng. 3 (1971) 575–586.
[13] Z.-C. Shi, A convergence condition for the quadrilateral Wilson element, Numer. Math. 44 (1984) 349–361.
[14] R.L. Taylor, F. Auricchio, Linked interpolation for Reissner–Mindlin plate elements: Part II—a simple triangle, Int. J. Numer. Methods Eng. 36 (1993) 3057–3066.
[15] T.-X. Zhou, Stabilized hybrid finite element methods based on the combination of saddle point principles of elasticity problems, Math. Comput. 72 (2003) 1655–1673.
[16] T.-X. Zhou, Y.-F. Nie, Combined hybrid approach to finite element schemes of high performance, Int. J. Numer. Methods Eng. 51 (2001) 181–202.
[17] T.-X. Zhou, X.-P. Xie, Zero energy-error mechanism of the combined hybrid method and improvement of Allman's membrane element with drilling d.o.f.'s, Commun. Numer. Methods Eng. 20 (2004) 241–250.
[18] Z. Wang, B. Hu, Research of combined hybrid method applied in the Reissner–Mindlin plate model, Appl. Math. Comput. 182 (2006) 49–66.
[19] S.L. Weissman, R.L. Taylor, Resultant field for mixed plate bending elements, Comput. Methods Appl. Mech. Eng. 79 (1990) 321–355.
[20] C.-C. Wu, M.-G. Huang, T.H.H. Pian, Consistency condition and convergence criteria of incompatible elements: general formulation of incompatible functions and its application, Comput. Struct. 27 (1987) 639–644.
[21] Z. Xu, O.C. Zienkiewicz, L.F. Zeng, Linked interpolation for Reissner–Mindlin plate elements: Part III—an alternative quadrilateral, Int. J. Numer. Methods Eng. 37 (1994) 1437–1443.
[22] Z. Zhang, S. Zhang, Wilson's element for the Reissner–Mindlin plate, Comput. Methods Appl. Mech. Eng. 113 (1994) 55–65.
[23] O.C. Zienkiewicz, Z. Xu, L.F. Zeng, A. Samuelsson, N.-E. Wiberg, Linked interpolation for Reissner–Mindlin plate elements: Part I—a simple quadrilateral, Int. J. Numer. Methods Eng. 36 (1993) 3043–3056.
[24] O.C. Zienkiewicz, R.L. Taylor, J. Too, Reduced integration technique in general analysis of plates and shells, Int. J. Numer. Methods Eng. 3 (1971) 275–290.
[25] O.C. Zienkiewicz, R.L. Taylor, Finite Element Method Solid Mechanics, vol. 2, fifth ed., Butterworth-Heinemann, London, 2000.